Available online at www.sciencedirect.com

ScienceDirect

Geochimica et Cosmochimica Acta 122 (2013) 478–497

Geochimica et Cosmochimica Acta

www.elsevier.com/locate/gca

Natural age dispersion arising from the analysis of broken crystals. Part I: Theoretical basis and implications for the apatite (U–Th)/He thermochronometer ☆

Roderick W. Brown [a,*], Romain Beucher [a], Steven Roper [b], Cristina Persano [a], Fin Stuart [c], Paul Fitzgerald [d]

[a] School of Geographical and Earth Sciences, University of Glasgow, Lilybank Gardens, Glasgow, G12 8QQ, UK
[b] School of Mathematics and Statistics, University of Glasgow, 15 University Gardens, Glasgow, G12 8QW, UK
[c] Scottish Universities Environmental Research Center, Rankine Avenue, Scottish Enterprise Technology Park, East Kilbride, G75 0QF, UK
[d] Department of Earth Sciences, Syracuse University, 204 Heroy Geology Laboratory, Syracuse, NY 13244-1070, USA

Received 5 November 2012; accepted in revised form 30 May 2013; available online 11 June 2013

Abstract

Over the last decade major progress has been made in developing both the theoretical and practical aspects of apatite (U–Th)/He thermochronometry and it is now standard practice, and generally seen as best practice, to analyse single grain aliquots. These individual prismatic crystals are often broken and are fragments of larger crystals that have broken during mineral separation along the weak basal cleavage in apatite. This is clearly indicated by the common occurrence of only 1 or no clear crystal terminations present on separated apatite grains, and evidence of freshly broken ends when grains are viewed using a scanning electron microscope. This matters because if the ^{4}He distribution within the whole grain is not homogeneous, because of partial loss due to thermal diffusion for example, then the fragments will all yield ages different from each other and from the whole grain age. Here we use a numerical model with a finite cylinder geometry to approximate ^{4}He ingrowth and thermal diffusion within hexagonal prismatic apatite crystals. This is used to quantify the amount and patterns of inherent, natural age dispersion that arises from analysing broken crystals. A series of systematic numerical experiments were conducted to explore and quantify the pattern and behaviour of this source of dispersion using a set of 5 simple thermal histories that represent a range of plausible geological scenarios. In addition some more complex numerical experiments were run to investigate the pattern and behaviour of grain dispersion seen in several real data sets. The results indicate that natural dispersion of a set of single fragment ages (defined as the range divided by the mean) arising from fragmentation alone varies from c. 7% even for rapid (c. 10 °C/Ma), monotonic cooling to over 50% for protracted, complex histories that cause significant diffusional loss of ^{4}He. The magnitude of dispersion arising from fragmentation scales with the grain cylindrical radius, and is of a similar magnitude to dispersion expected from differences in absolute grain size alone (spherical equivalent radii of 40–150 μm). This source of dispersion is significant compared with typical analytical uncertainties on individual grain analyses (c. 6%) and standard deviations on multiple grain analyses from a single sample (c. 10–20%). Where there is a significant difference in the U and Th concentration of individual grains (eU), the effect of radiation damage accumulation on ^{4}He diffusivity (assessed using the RDAAM model of Flowers et al. (2009)) is the primary cause of dispersion for samples that have experienced a protracted thermal history, and can cause dispersion in excess of 100% for realistic ranges of eU concentration (i.e. 5–100 ppm). Expected natural dispersion arising from the combined effects of reasonable variations in grain size (radii 40–125 μm), eU concentration (5–150 ppm) and fragmentation would typically exceed 100% for complex thermal histories. In addition to adding a significant component of natural dispersion

☆ This is part I of previously published article entitled "Natural age dispersion arising from the analysis of broken crystals, Part II. Practical application to apatite (U-Th)/He thermochronometry" published in issue 120, pages 395-416 (doi:10.1016/j.gca.2013.05.042).

* Corresponding author.
E-mail address: roderick.brown@glasgow.ac.uk (R.W. Brown).

http://dx.doi.org/10.1016/j.gca.2013.05.041

to analyses, the effect of fragmentation also acts to decouple and corrupt expected correlations between grain ages and absolute grain size and to a lesser extent between grain age and effective uranium concentration (eU). Considering fragmentation explicitly as a source of dispersion and analysing how the different sources of natural dispersion all interact with each other provides a quantitative framework for understanding patterns of dispersion that otherwise appear chaotic. An important outcome of these numerical experiments is that they demonstrate that the pattern of age dispersion arising from fragmentation mimics the pattern of ^{4}He distribution within the whole grains, thus providing an important source of information about the thermal history of the sample. We suggest that if the primary focus of a study is to extract the thermal history information from (U–Th)/He analyses then sampling and analytical strategies should aim to maximise the natural dispersion of grain ages, not minimise it, and should aim to analyse circa 20–30 grains from each sample. The key observations and conclusions drawn here are directly applicable to other thermochronometers, such as the apatite, rutile and titanite U–Pb systems, where the diffusion domain is approximated by the physical grain size.

1. INTRODUCTION

All geological radiometric dating techniques depend on the accumulation of a daughter product produced by radioactive decay of a parent nuclide. When accumulation begins is largely a function of temperature, as the daughter radionuclides will not be retained at high temperatures because the process of thermally activated diffusion enables them to move freely and escape from the mineral grain or rock in which they are being formed (e.g. Jäger and Hunziker, 1979; McDougall and Harrison, 1999; Faure and Mensing, 2005). If a rock cools quickly, after crystallisation from a magma for example, and resides at low temperatures then the radiometric age will reflect the time of crystallisation, and thus provide a good estimate of the age of the rock. In cases where the rocks have experienced a complex thermal history, the radiometric ages usually reflect the samples' prolonged temperature-time trajectory through the zone of partial retention and therefore do not date a discrete geological event, such as the time of crystallisation of an igneous rock (e.g. Harrison et al., 2005; Ehlers et al., 2005; Blackburn et al., 2011). This behaviour is typical of most low temperature systems such as apatite fission track and (U–Th)/He thermochronometry and these techniques have proved to be extremely useful for reconstructing complex thermal histories of geological samples (e.g. Gallagher et al., 1998; Reiners et al., 2005). In the last decade or so apatite (U–Th)/He thermochronometry in particular has emerged as an important tool for quantifying the cooling history of rocks as they pass through the upper 1–3 km of the crust. The thermal sensitivity of this technique (circa 30–90 °C) has gained the interest of a wide range of Earth scientists because it is applicable to interdisciplinary studies in landform evolution, structural geology, and geodynamics (e.g. Reiners et al., 2005; Reiners and Brandon, 2006).

The key challenge in interpreting the measured ages obtained using thermochronometry techniques is how to identify and then interpret samples that have experienced significant partial loss of daughter product because of thermal diffusion. This is difficult because the age measured for a given mineral grain is effectively determined by the volume integral of the daughter product concentration over the diffusion domain, so many different spatial distributions arising from different possible thermal histories are able to generate the identical integral and hence identical age. A single age will therefore be consistent with a number of possible thermal histories, and so the thermal history information recorded by a single age determined on one grain from a sample is ambiguous. The dilemma for thermochronologists is that knowing only the age of a single whole grain is insufficient for determining a unique thermal history, because what is actually needed is a measure of the spatial distribution of the daughter product concentration within the grain, i.e. the shape of the daughter product diffusion profile. An innovative step heating technique applied to apatite (U–Th)/He thermochronometry that utilises the addition of a uniform reference concentration of ^{3}He, produced by proton irradiation of the sample, can be used to extract the thermal history information encoded in the spatial pattern of the concentration of helium within a single apatite grain (Shuster and Farley, 2004; Shuster, 2005). By measuring the ^{4}He/^{3}He ratio of the step wise released gas it is possible to retrieve the pattern of ^{4}He distribution within the crystal and hence place robust constraints on the likely thermal history of the sample. For this technique to work reliably it is necessary to analyse whole and intact crystals that have not been broken during mineral separation procedures (Farley et al., 2010).

The majority of apatite (U–Th)/He thermochronometry studies still make use of the conventional approach of analysing a small number of single grain aliquots, typically 3–6, and totally degassing each grain individually using a single laser heating step (Reiners et al., 2005; Farley, 2002). In these studies single apatite grains selected for analysis are often fragments of larger crystals that were broken (Fig. 1), typically parallel to the basal cleavage direction in apatite, during the mineral separation process (Farley, 2002; Farley et al., 2010). Many of these studies have also shown that the range of single grain ages obtained from a single rock sample are more dispersed than expected considering only the analytical uncertainties (e.g. Fitzgerald et al., 2006; Kohn et al., 2009; Flowers and Kelley, 2011). This dispersion arises from both natural causes, which are inherent to the ideal system, and which are helpful from a thermochronometry point of view and also from other causes that are imposed on, or extraneous to, the ideal system and which are usually unhelpful. For the ideal system we mean that the apatite grains being analysed are whole, intact, idiomorphic crystals which all have a uniform distribution of U and Th and are devoid of any U and Th bearing exsolution phases and/or mineral and fluid inclusions. These common and often complex patterns of age

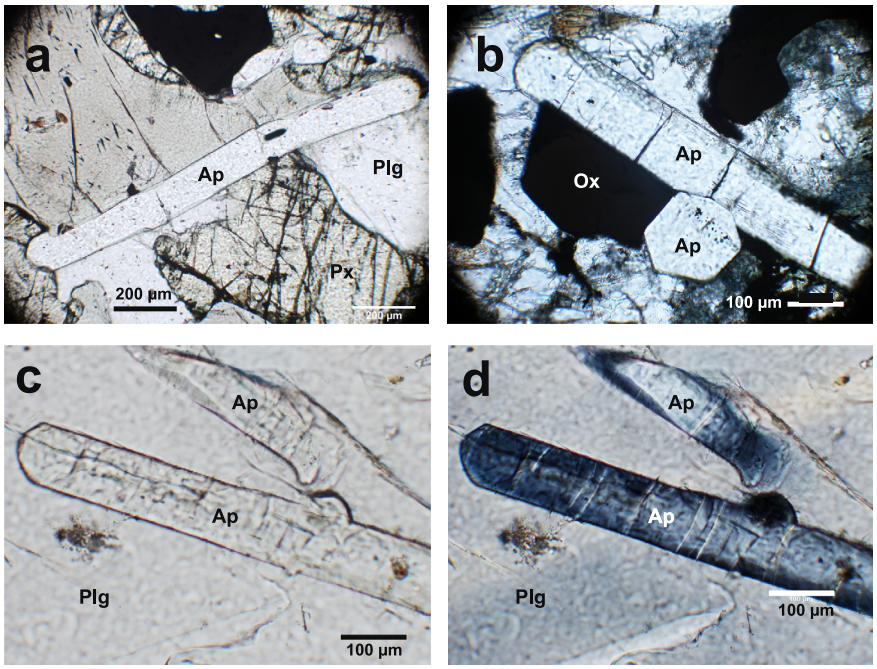

Fig. 1. Photomicrographs of rock thin sections for a medium grained gabbro sample from the Bushveld Complex, South Africa (BK1-650 m) that illustrate the typical natural habit and basal cleavage of apatite. Ap, apatite; Px, pyroxene; Plg, plagioclase; Ox, Fe-oxides. (a) An example of a large, twinned apatite crystal which would likely break in three places on extraction. (b) Elongated, prismatic crystal showing clear fractures parallel to 001 basal cleavage direction. Although some fractures may be natural, most are caused during the thin section grinding and polishing processes. (c) Elongated prismatic apatite crystal in plane light and, (d) in polarised light. Note the numerous fractures perpendicular to the *c*-axis (thin white lines) which are highlighted by refraction in polarised light.

dispersion frustrate the interpretation and derivation of reliable thermal history information from such data.

The main purpose of this paper is to examine and to quantify the pattern of age dispersion that arises from the routine analysis of fragments of broken crystals. We also document how this source of natural dispersion compares and interacts with other causes to produce the magnitude and style of dispersion commonly seen in real data, and helps to explain dispersion behaviour that otherwise appears chaotic. Here we focus on the apatite (U–Th)/He thermochronometer and demonstrate additionally that, rather than adding additional "noise", natural dispersion arising from fragmentation contains useful information about the spatial distribution of ^{4}He within the previously whole grains and hence also about the thermal history of the host sample.

2. (U–Th)/He THERMOCHRONOMETRY AND SINGLE GRAIN AGE DISPERSION

2.1. Causes of inherent natural dispersion

A key parameter in all thermochronometry techniques is the size of the effective diffusion domain, and this may vary from mineral to mineral and even within a single grain for a given mineral (e.g. Lovera et al., 2002). This parameter is important because the closure temperature for a given system is dependent on the diffusivity and the size of the diffusion domain; the larger the diffusion domain the higher the closure temperature. Diffusion studies of He in apatite have demonstrated that for the (U–Th)/He thermochronometry technique the effective diffusion domain is the physical grain itself (Farley, 2000; Cherniak et al., 2009; van Soest et al., 2011). So, by analysing multiple grains with a range of grain sizes a sample's thermal history may be constrained because the smaller grains yield younger ages than the larger grains, and the pattern of this dispersion is a function of the sample's thermal history (Reiners and Farley, 2001). This effect can produce large amounts of dispersion of the order of 50–100% for effective spherical grain radii of c. 50–100 µm, depending on the thermal history. Here we define dispersion as the range divided by the mean of a set of single grain ages obtained from one sample, reported as a percentage. We use the range (i.e. *maximum age − minimum age*) as a simple statistic for quantifying dispersion, rather than the standard deviation of the mean, because the distribution of fragment ages is often strongly skewed and so the standard deviation is not an accurate estimate of the dispersion.

If the rate of diffusion of the daughter nuclide within single grains from the same sample varies in a quantitative and known way, then this too can be exploited to obtain constraints on the thermal history. The rate of diffusion may be a function of the mineral chemistry, as it is for the annealing of fission tracks in apatite (e.g. Carlson et al., 1999; Ketcham et al., 2007), or the physical nature of the lattice. Accumulation of radiation damage in apatite for example has been shown to effect the diffusivity of ^{4}He, with lower rates of diffusion measured for apatites with higher densities of accumulated radiation damage (Shuster et al., 2006). The effect of this phenomenon has been included in thermal history models that account for the temporal variation in ^{4}He diffusivity arising from the natural

accumulation and annealing of radiation damage (e.g. Flowers et al., 2007, 2008, 2009; Gautheron et al., 2009). So, in addition to dispersion arising from physical grain size variations, differences in concentration of U and Th can assist in constraining the thermal histories of samples because grains with higher eU (i.e. [U] + 0.235[Th]) yield older ages than grains with lower eU for the same thermal history (e.g. Flowers et al., 2007; Flowers, 2009; Kohn et al., 2009; Flowers and Kelley, 2011). The effects of radiation damage can cause very large differences in age for some thermal histories, exceeding 200% in some cases, if there is a significant difference in the eU content of individual grains, and so when present this type of dispersion provides excellent constraints on the range of viable thermal histories (e.g. Gautheron et al., 2009; Flowers et al., 2009).

It is now standard practice to assess and analyse the dispersion of conventional single grain (U–Th)/He ages for a given sample by looking for the expected positive correlations between grain age and grain size and/or eU (e.g. Ault et al., 2009; Kohn et al., 2009; Flowers et al., 2009; Flowers and Kelley, 2011). In these plots the size of a prismatic grain is usually represented using the spherical equivalent radius transformation, which determines an effective spherical equivalent radius, referred to here as R^*, for a sphere with the same volume/surface-area ratio as the actual grain (e.g. Farley, 2002; Meesters and Dunai, 2002b). Positive correlations between these parameters are typically interpreted as evidence for a complex thermal history and this information can be used to help constrain estimates of likely thermal histories. The lack of any correlation is equivocal however, and could imply simple rapid cooling or possibly over dispersion arising from other sources. It is not uncommon for there to be only a weak correlation, or none at all, between the measured grain age and the spherical equivalent grain size (R^*) and/or eU, and for the amount of age dispersion to be larger than expected (e.g. Fitzgerald et al., 2006; Kohn et al., 2009; Flowers and Kelley, 2011). This issue is discussed in more detail below.

2.2. Causes of imposed extraneous dispersion

2.2.1. Heterogeneous U and Th distribution

Because of the long stopping distance for α-particles within apatite a significant proportion of ^{4}He atoms are ejected directly from the outer 20 μm or so of the grain (Farley et al., 1996; Ketcham et al., 2011; Gautheron et al., 2012). If the source is heterogeneously distributed then more or less ^{4}He is ejected than expected from a uniform distribution. Grains with more U and Th in the core will retain more ^{4}He than expected and consequently yield older ages than grains with high U and Th in the outer rim (c. 20 μm) which will lose more ^{4}He than expected and yield younger ages relative to a uniform distribution. The rate of ^{4}He diffusion may also be affected by U and Th zonation in two ways; firstly because of differences in the ^{4}He concentration gradient caused by the heterogeneous source distribution and secondly because radiation damage accumulation will also be heterogeneous for zoned grains thus causing spatial differences in ^{4}He diffusivity within the grain. These effects can interact in complex ways. For example, grains with higher eU in the rims, compared with the core, will accumulate more radiation damage and be more retentive and retard ^{4}He diffusion out of the grain thus counteracting the enhanced loss of helium due to α-ejection (Farley et al., 2011; Ault and Flowers, 2012). The behaviour and magnitude of this source of dispersion has been investigated in some detail both theoretically (Meesters and Dunai, 2002a; Farley et al., 2011) and experimentally for samples from Antarctica (Fitzgerald et al., 2006) and northern Canada (Ault and Flowers, 2012). These studies indicate that while this mechanism could theoretically generate 30–40% dispersion for some thermal histories and extreme heterogeneity, for typical patterns of heterogeneity of U and Th, dispersion from this cause is unlikely to exceed of 10–15%, and for practical thermochronometry purposes assuming a uniform concentration of U and Th is unlikely to cause significant problems unless the heterogeneity is extreme (Fitzgerald et al., 2006; Farley et al., 2011; Ault and Flowers, 2012).

2.2.2. Mineral and fluid inclusions

The presence of high [U] and [Th] micro-inclusions and/or He bearing fluid inclusions have been cited as the possible cause of observed 'excess' age dispersion within some samples (e.g. Lippolt et al., 1994; House et al., 1997; Farley, 2002; Fitzgerald et al., 2006). Apatite grains of a suitable size and with good crystal shape are now carefully selected and handpicked under high magnification using a binocular microscope, and are usually also subsequently screened under polarised light microscopy for the presence of small mineral and/or fluid inclusions. However in some cases it is possible that the presence of tiny, very high U and Th bearing inclusions (e.g. monazite, zircon) or microscopic exsolution lamellae of monazite may be missed (Farley and Stockli, 2002). Routine procedures for the dissolution of apatite will not dissolve these inclusions and so the U and Th contained within these inclusions will not be measured, but the ^{4}He produced by them will be, and so the ages will be anomalously old. Careful theoretical calculation and experimental work by Vermeesch et al. (2007) has shown that the contribution by mineral inclusions to the age of a grain is likely to be very small (< a few %) unless the inclusions are quite large (< 0.1 of the grain size) and/or have an unusually high U and Th content (i.e. >1000 times that of the apatite). With careful screening and handpicking using optical microscopy, augmented where warranted by scanning electron microscopy for problematic samples, the routine significance of this possible source of dispersion is unlikely to exceed a few percent, and is normally insignificant (Farley, 2002; Vermeesch et al., 2007).

2.2.3. He implantation

The corollary of ejection of ^{4}He from the host apatite due to long stopping distance for α-particles is the implantation of ^{4}He from outside the apatite grain. ^{4}He implantation may occur from high U and Th bearing accessory minerals like monazite or zircon being adjacent to the apatite grain (acting as 'bad neighbours') within the host

rock or may arise from high U and Th bearing mineral coatings like Fe–Mn oxide coatings (Murray et al., 2011). This possible source of dispersion has also been investigated in some detail both theoretically (Gautheron et al., 2012) and experimentally (Spiegel et al., 2009). The theoretical work indicates that for realistic U and Th concentrations, abundances and sizes of accessory minerals, this source of excess ^{4}He is unlikely to be significant on a routine basis. In some circumstances, where a rock has abundant, large (i.e. similar in size to the apatite grains) and high U and Th bearing accessory minerals (i.e. 20× that of the of apatite being dated) it may be a problem. For example, an apatite grain would yield an age that was circa 60% older than normal if it had a single large (i.e. > 0.3× apatite grain size) 'bad neighbour', and up to 300% older if the apatite was effectively surrounded by zircon or monazite. These estimates assume that the 'bad neighbours' are in direct contact (i.e. within 1–2 μm of the apatite) and would diminish with increasing distance. For most rocks with normal abundances and size distributions of accessory phases this effect is likely to be rare, simply because the probability of it occurring to a given grain is low and the probability of that particular grain being picked for dating even lower. This effect may well explain occasional individual 'rogue' analyses that are much older than any other grain in the sample, sometimes even older than the crystallization age of the rock itself, which is difficult to explain by any other process.

2.3. Dispersion arising from analysing broken crystals

Apatite crystals typically occur in natural samples with a hexagonal prismatic habit and display a weak basal cleavage, parallel to 001, which predisposes grains to being broken at right angles to their prismatic axes (Fig. 1). Apatite crystals routinely analysed in the laboratory are therefore often fragments of larger, whole grains that existed in the rock prior to extraction by mineral separation processes (Farley et al., 1996, 2010; Farley, 2002). The sharp, clean fractures displayed when viewed using scanning electron microscopy clearly show that the grains are broken during mineral separation (Fig. 2). In these cases an adjustment needs to be made to the F_T correction factor (Farley et al., 1996; Ketcham et al., 2011; Gautheron et al., 2012) to account for the broken faces of crystals because no α-ejection will have occurred through the broken faces. The routine practice in most laboratories is to multiply the length of a broken crystal by a factor of 1.5 for this purpose unless the grains are demonstrably unbroken (Farley, 2002). More sophisticated options for calculating the F_T correction factor that considers the full geometry of grains as well as heterogeneous U and Th is possible (Ketcham et al., 2011; Gautheron et al., 2012). However, this practice only effects the calculation of the corrected age (i.e. age corrected for α-ejection), and is usually not extended to modifying the raw grain ages or to the calculation of the effective spherical equivalent radii, R^*, of fragments for use in modelling the thermal histories of samples. The differences between the R^* values for fragments (without any correction applied) compared with the R^* values for the whole grains from which they were derived can be large, i.e. circa 20–50% (see fragment lists provided in the Electronic annex).

If the spatial distribution of the daughter and parent nuclides are perfectly uniform, such as might be expected for a sample that cooled rapidly through the partial retention zone, then it is not critical whether the grains being analysed are broken or not, because the volume ratio of daughter to parent will remain intact and the measured age will remain unchanged. However, if the sample has experienced significant partial loss of ^{4}He by thermal diffusion then the spatial distribution of ^{4}He within the crystal will not be uniform, and will vary from a maximum in the core to zero at the grain boundaries (Fig. 2). In this case if broken crystals are analysed then an additional source of dispersion is introduced because different sized fragments of an initially whole grain will contain different volume ratios of daughter to parent nuclides and hence will yield different ages. We refer to this source of dispersion as inherent natural dispersion because it occurs as a natural consequence of common breakage of otherwise ideal grains. In the following sections we demonstrate that this source of dispersion is significant and that it contains useful information about the distribution of ^{4}He within the originally intact whole grain, and therefore can be exploited to constrain the thermal history of the sample. We also analyse why this source of dispersion acts to decouple the expected relationships between grain age and grain size (R^*) and between grain age and eU.

3. QUANTIFYING THE NATURAL DISPERSION ARISING FROM THE ANALYSIS OF BROKEN CRYSTALS

To investigate and quantify the effects of analysing fragments of larger crystals we use a simple model for calculating the simultaneous ingrowth and thermal diffusion of ^{4}He within a finite cylinder geometry for an arbitrary thermal history. The basic assumptions made and mathematical approach is similar to previous work in this area by Meesters and Dunai (2002a,b) and Watson et al. (2010). The important difference in our model is that it enables us to explicitly deal with whole crystals as well as fragments having either 1 or no terminations. A full description of the model including details about implementation and example source code are provided in a companion paper (Beucher et al., 2013 this volume).

3.1. Model description

The hexagonal prismatic geometry of typical apatite crystals is well represented by the form of a finite cylinder (Fig. 2). The geometry of the grain is then specified by the cylindrical radius and the length of the cylinder which has flat terminations. We assume that the ^{4}He concentration is initially zero everywhere and is always zero at the surface of the crystal and that the ^{4}He has a spatially uniform source (i.e. [U] and [Th]) distributed throughout the cylinder. The effect of α-ejection is explicitly included by modifying the source term to account for the fraction of ^{4}He lost during each time step following

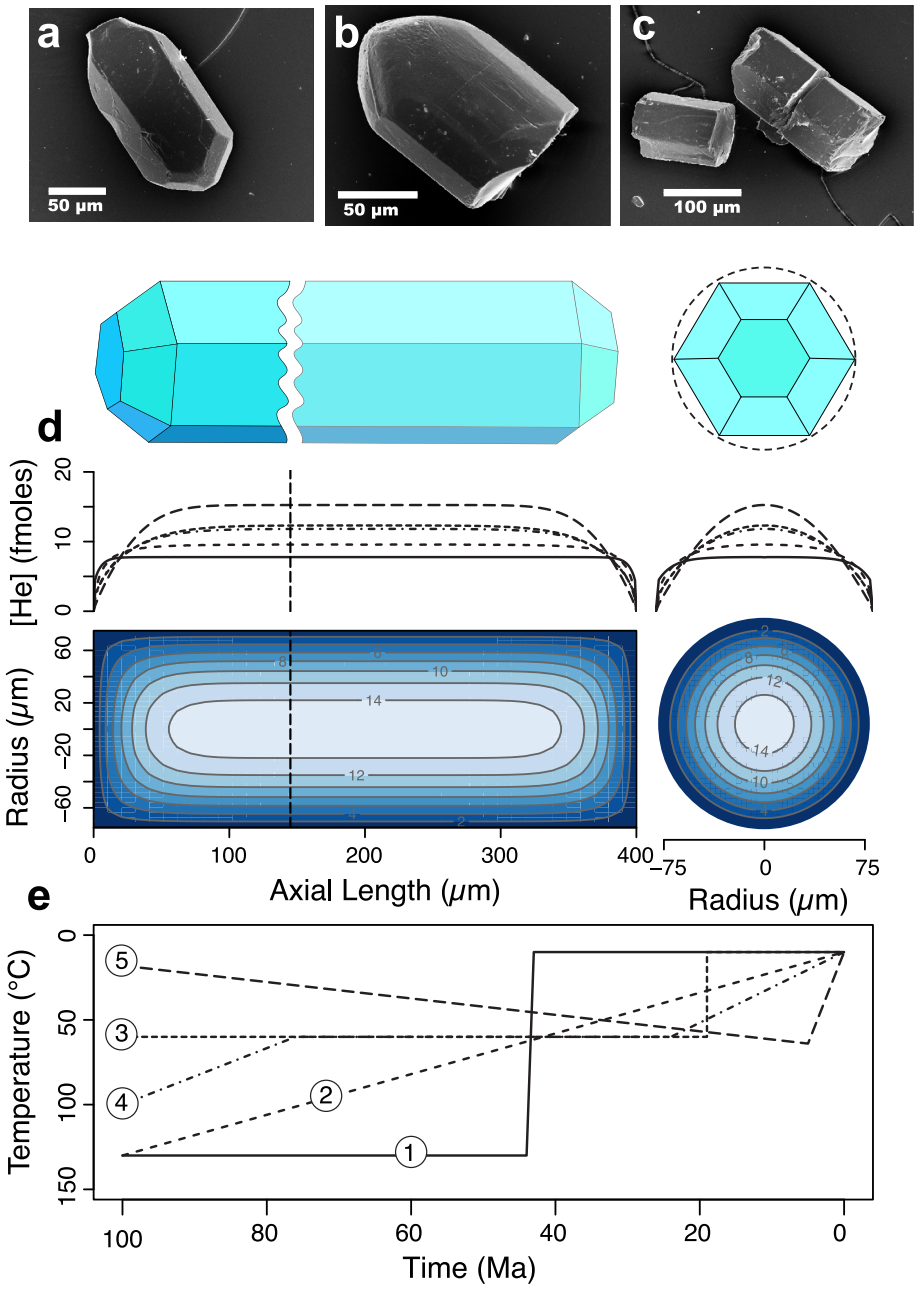

Fig. 2. Summary of the numerical model geometry and design and three example Scanning Electron Microscopy (SEM) images of apatite crystals separated from the same gabbro sample as shown in Fig. 1. Idiomorphic whole grain (2T grain), (b) broken crystal with 1 termination (1T grain) and (c) broken grains with no terminations (0T grains). (d) Model axial and radial helium diffusion profiles generated for the 5 model thermal histories used in the experiments ($D_o = 0.00316 m^2/s, E_a = 138 kJ/mol$). The contoured panels illustrate the spatial distribution of helium (in femto moles/m^3) within an axial and a radial slice through a cylinder (length = 400 µm, radius = 75 µm, [U] = 20 ppm, [Th] = 20 ppm) for the WOLF-5 thermal history. (e) The T–t graphs for the 5 model thermal histories used in the experiments and referred to here as WOLF-1 to 5 in the text.

the approach proposed by Meesters and Dunai (2002b). We use the Durango apatite ^{4}He diffusion parameters ($D_0 = 0.00316\ m^2/s, E_a = 138\ kJ/mol$) of Farley (2000) and to simulate the effect of radiation damage accumulation and annealing on the helium diffusivity (Gautheron et al., 2009; Flowers et al., 2009) we have included the RDAAM model described by Flowers et al. (2009). After any given arbitrary thermal history the AHe age of a whole grain with 2 terminations (2T grain) is then simply calculated by performing the volume integral of the ^{4}He concentration over the whole grain. The AHe ages of model fragments derived from a larger crystal are determined by first calculating the He distribution for the initial whole crystal geometry and then performing the volume integral of the

^{4}He concentration for the fragment over the appropriate limits along the axial length. So for fragments with 1 termination (1T grain) the integration is performed from one end of the crystal to the end of the fragment and for grains with no terminations (0T grains) between the ends of the fragment.

We investigated the fragmentation effect for a range of thermal history styles representing a range of typical geological scenarios. These histories are the same as those used initially by Wolf et al. (1998) and we refer to them as WOLF-1 to WOLF-5 respectively (Fig. 2e). These histories provide an ideal basis for this discussion because they all yield similar AHe ages for a standard grain size but clearly produce very different spatial patterns of ^{4}He concentration within the grains (Fig. 2d) which display different degrees of 'rounding' of both the axial and radial ^{4}He diffusion profiles.

The effect of α-ejection within the outer 20 μm or so of the crystal also leads to 'rounding off' of the ^{4}He profile, and this is most significant for thermal histories which have experienced little loss of ^{4}He due to thermal diffusion such as WOLF-1 which involves instantaneous cooling from high temperatures to low temperatures (Fig. 3). As illustrated though in Fig. 3, even moderate amounts of thermal diffusion (e.g. WOLF-2) cause the shape of the diffusion profile to change over a much longer distance (equivalent to the cylindrical radius) than the stopping distance characteristic of α-ejection (i.e. circa 20 μm). Furthermore, with increased amounts of diffusional loss (e.g. WOLF-5) it is clear that the effects of α-ejection become insignificant because all the helium that was lost by ejection would have been lost anyway because of thermal diffusion. This effect has been nicely quantified elsewhere by Gautheron et al. (2012) where they showed that if the standard F_T correction (Farley et al., 1996) is made to samples that have experienced severe thermal diffusion then the 'corrected' AHe ages will always be too old (typically by 3–8%).

However, in this study we are only concerned with modelling the AHe ages which include the loss of helium caused by α-ejection accumulated over the history of the sample. These ages are equivalent to the so called 'uncorrected' or raw ages measured in the laboratory, and they are the appropriate measurements to use for constraining thermal history modelling aimed at deriving the unknown thermal history of a sample. We first examine in detail the effect of fragmentation alone followed by consideration of the combined effects of both fragmentation and variable grain size and then finally the combined effects including radiation damage.

3.2. Model results

Our initial numerical experiments involved generating random sets of 1T and 0T fragments for each of the five thermal histories (i.e. WOLF-1 to 5), with all fragments being derived from an initial grain with the same geometry and size. Comprehensive details of all fragments, including dimensions, eU concentrations and calculated ages, for all the experiments are included in the Electronic annex. This standard initial grain had a length of 400 μm and a cylindrical radius of 75 μm and a nominal [U] and [Th] concentration of 20 ppm. The resulting axial ^{4}He concentration profiles (Fig. 4a) and the patterns of fragment AHe age dispersion obtained for each thermal history are presented on age dispersion fragment distribution (ADFD) plots (Fig. 4b) and as conventional probability distribution diagrams (Fig. 4c). The ADFD plots (Fig. 4b) nicely illustrate the systematic pattern of age dispersion as a function of the fragment lengths, and emphasise the difference in these patterns between the 1T and 0T fragments.

The total amount of dispersion increases systematically with increasing amounts of thermal diffusion, i.e. from very little dispersion for WOLF-1 (c. 7%) through to severe dispersion for WOLF-5 (c. 50%). This increase in dispersion reflects the increasing loss of helium by axial diffusion through the ends of the whole grains for steadily increasing total amounts of helium loss. This is reflected by the progressive increase in 'rounding off' of the axial diffusion profiles at the ends of the grains as illustrated by the five WOLF histories (Fig. 4a). The 1T fragments in all cases follow a similar trajectory with their ages initially increasing (relative to the whole grain age) with decreasing fragment length, reaching a maximum age for fragment lengths of circa $L_0 - R_0$, then decreasing steadily to significantly younger ages for shorter fragment lengths (where L_0 is the whole grain length and R_0 is the grain radius).

In contrast, most of the 0T fragment ages (which are typically derived from the centre of the whole crystal) initially increase with decreasing fragment length, asymptotically reaching a maximum 'plateau age' which is older than the true whole grain age, for fragment lengths which are $\leqslant L_0 - 2R_0$. This behaviour reflects the fact that the fragments on the plateau are missing both the terminations, where the ^{4}He concentration is the lowest, and so yield consistent and anomalously old ages. The 0T fragments that yield ages that fall between this plateau age and the trajectory defined by the 1T grains are fragments that were derived from nearer the ends of the initial whole grains (i.e. one end of the fragment is $\leqslant R_0$ from a termination). These fragments have been effected by axial diffusion as well as radial diffusion and so behave in an intermediate fashion, yielding ages between that of a 'core' derived 0T fragment and a true 1T fragment.

The most important observation from these simple experiments is that the pattern of dispersion, especially for the 1T fragments, mimics the shape of axial ^{4}He diffusion profile (Fig. 4a). So for WOLF-1 where the axial ^{4}He diffusion profile is flat, the dispersion pattern on the ADFD plot (Fig. 4b) is also flat, while for WOLF-5 for example, the axial diffusion profile is strongly curved and so is the pattern of dispersion of the 1T fragment ages.

3.2.1. Age dispersion fragment distribution (ADFD) plots

To discuss these systematic patterns further let us look more closely at the WOLF-5 ADFD plot (Fig. 5). It is clear that the fragment ages obtained for 1T fragments with exactly half the initial length, $L_0/2$, are the same as for the whole grain, while fragments which are less than $L_0/2$ in length are younger and those that are longer than $L_0/2$ are older than the true whole grain age. The distinctive maximum in the 1T fragment age trajectory occurs for

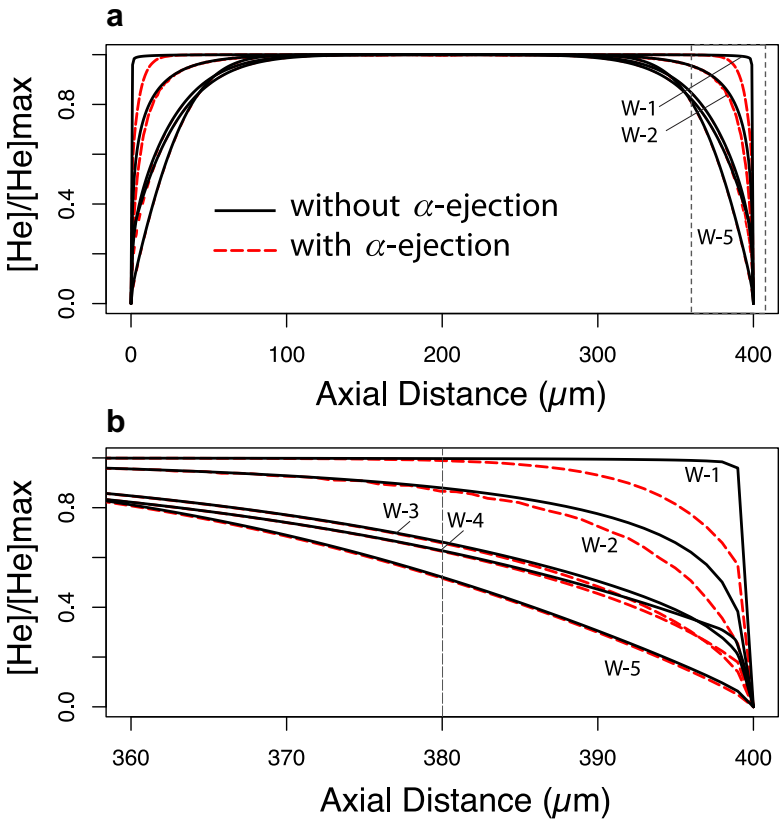

Fig. 3. The effect of α-ejection on the shape of the helium diffusion profiles. Plots of the axial helium diffusion profiles along a standard cylindrical grain, with a length of 400 μm and a radius of 75 μm and a nominal [U] and [Th] concentration of 20 ppm, for the 5 thermal histories used for the experiments ($D_o = 0.00316 m^2/s, E_a = 138 kJ/mol$). The black solid curves are for ingrowth and thermal diffusion only (no α-ejection) and the dashed-red curves include the effect of α-ejection added cumulatively throughout the thermal history. (a) Complete profiles and (b) enlarged section showing detail at one end of the crystal. The mean α stopping distance for apatite is shown in (b) by the thin dashed vertical line. (For interpretation of the references to colour in this figure legend, the reader is referred to the web version of this article.)

fragments with lengths between $L_0 - R_0$ and L_0. This pattern is explained by considering the effect of 'slicing' progressively larger pieces off of the right hand end of the initial grain, remembering that the radial component of diffusion is the same everywhere along the cylinder. Each slice would remove a small fraction from the right hand end of the grain, so that initially these slices would remove parts of the crystal with a lower amount of ^{4}He than the average in the remaining fragment so that the resulting fragment is effectively enriched in ^{4}He and so has an older age. Once the slices reach the 'shoulder' of the axial diffusion profile the progressive slices do not remove parts of the grain with lower ^{4}He, but rather start removing parts of the grain which have a constant and relatively higher ^{4}He content than the average for remaining fragment, and so the ages start to decrease as this component of the grain is systematically reduced in size. The rate of increase in age and subsequent decrease for the 1T fragments going from right to left on the ADFD plot is thus controlled directly by the shape of the axial diffusion profile.

The fragment age pattern for the 0T fragments is initially similar, but the important difference is that after initially increasing with decreasing fragment length the 0T fragments define a maximum plateau age (43.3 Ma) which is reached once fragments are less than $L_0 - 2R_0$ in length. This plateau age is set by the radial diffusion of ^{4}He loss and is a function of the cylindrical radius primarily, and simply reflects fragments that were derived from the interior of the grain where the axial diffusion profile is flat and so their age is not a function of their length. Importantly, the shortest 0T fragment ages can either have a minimum age or a maximum age, or anything in between. This simply depends on where along the long axis of the initial grain they were located, and in some cases the 0T fragments behave like 1T fragments because one of their broken ends was close to the initial termination of the whole grain. An interesting phenomenon for 0T fragments is that they would most likely yield reproducible ages (i.e. the plateau age), and this age would be older than the true age of the whole grain from which they were derived. Also, it is clear that similar sized 0T fragments could yield very different ages and similar ages could be obtained from 0T fragments with very different sizes (Fig. 5). This effect would clearly yield chaotic relationships on an age versus R^* plot.

Some other useful observations to highlight from this analysis are that the mean age for the 0T fragments (41.9 Ma) is older than the true whole grain age (38.5 Ma). This is because the probability of deriving a 0T fragment

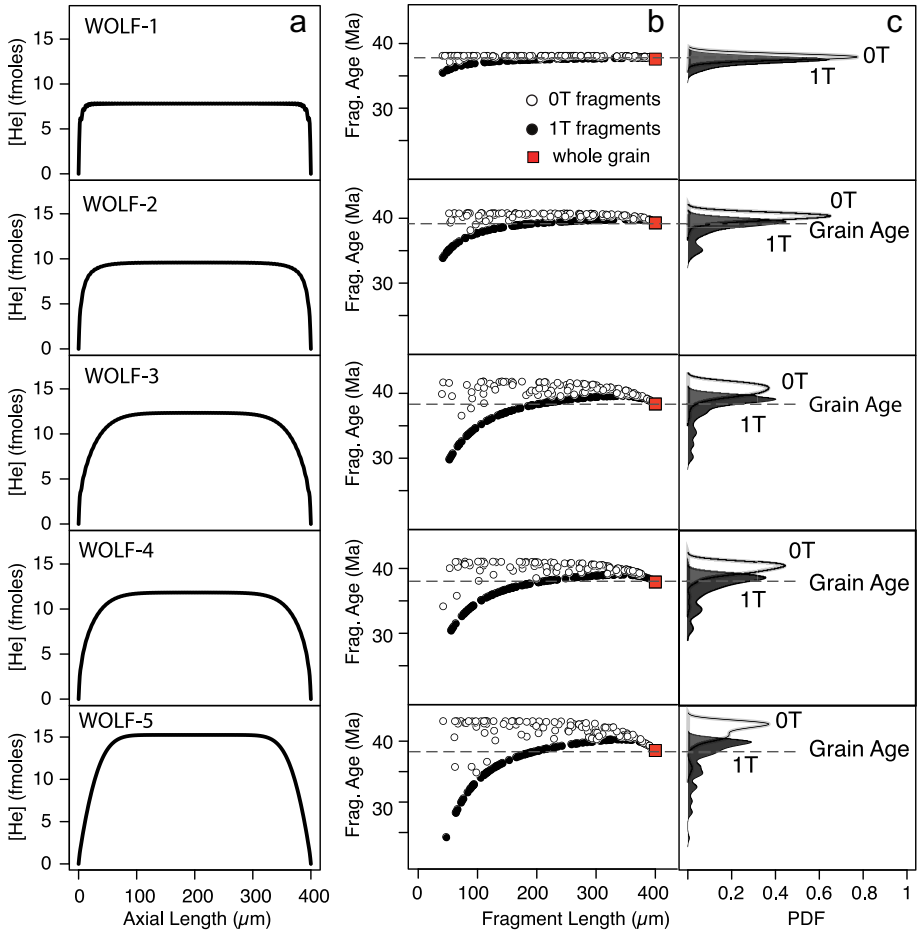

Fig. 4. Age dispersion fragment distribution (ADFD) plots for each of the five model thermal histories. (a) Axial helium diffusion profiles within a single standard grain (length of 400 μm and a radius of 75 μm and a nominal [U] and [Th] concentration of 20 ppm) for each of the 5 thermal histories. (b) ADFD plots for each history in which the fragment age is plotted against the fragment length (measured along the *c*-axis) for a random set of fragments 'cut' from the standard grain (red square). Fragments with 1 termination (1T grains) are shown as filled black circles and fragments with no terminations (0T grains) as white circles. The whole grain age (2T grain) is marked by the horizontal dashed line. Detailed fragment lists for each plot are included in the Electronic Annex. (c) Probability density plots illustrating the pattern of age dispersion for the 1T fragments (black curve) and 0T fragments (white curve). Note that the degree of dispersion increases with increasing diffusional loss of helium. The amount of dispersion increases as the 'roundness' of the axial diffusion profile increases, progressing from a minimum for the WOLF-1 history (rapid cooling with 'flat' diffusion profile) through to a maximum for WOLF-5. Also, an important observation is that the shape of the 1T dispersion pattern (black filled circles) on the ADFD plots shown in panel (b) mimics the shape of axial helium diffusion profiles shown in panel (a). (For interpretation of the references to colour in this figure legend, the reader is referred to the web version of this article.)

from the core of the whole grain (where the ^{4}He concentration is highest) is higher than it is from near the tips of the grain. The mean age for the 1T fragments (37.5 Ma) is slightly younger while the combined mean (for both 1T and 0T fragments, 39.7 Ma) is slightly higher but both are quite similar to the true whole grain age. So while this relationship depends on the actual and relative number, size, type and distribution of fragments it does provide some insight into why in some cases the mean age for a population of AHe ages may approximate the expected AHe age of a sample relative to other thermochronometry systems (e.g. Fitzgerald et al., 2006), although in that study the preferred or most representative age for the AHe age population lay between the minimum age and the weighted mean age.

3.2.2. Fragmentation and absolute grain size

To investigate the kind of dispersion patterns that might be observed for real data requires consideration of the other sources of natural dispersion in addition to fragmentation, and importantly how they interact with each other. To illustrate the consequences of including the effect of absolute grain size and differences in aspect ratio of the initial grains we ran experiments for all of the WOLF thermal histories where we generated 0T and 1T random fragments from a systematic set of 10 initial whole grains with lengths of 150, 300 and 400 μm and cylindrical radii of 50, 75, 100, and 150 μm which give L/R ratios between 2 and 8, and with [U] and [Th] concentrations of 20 ppm. The resulting ADFD plot for the WOLF-5 history is shown in Fig. 6

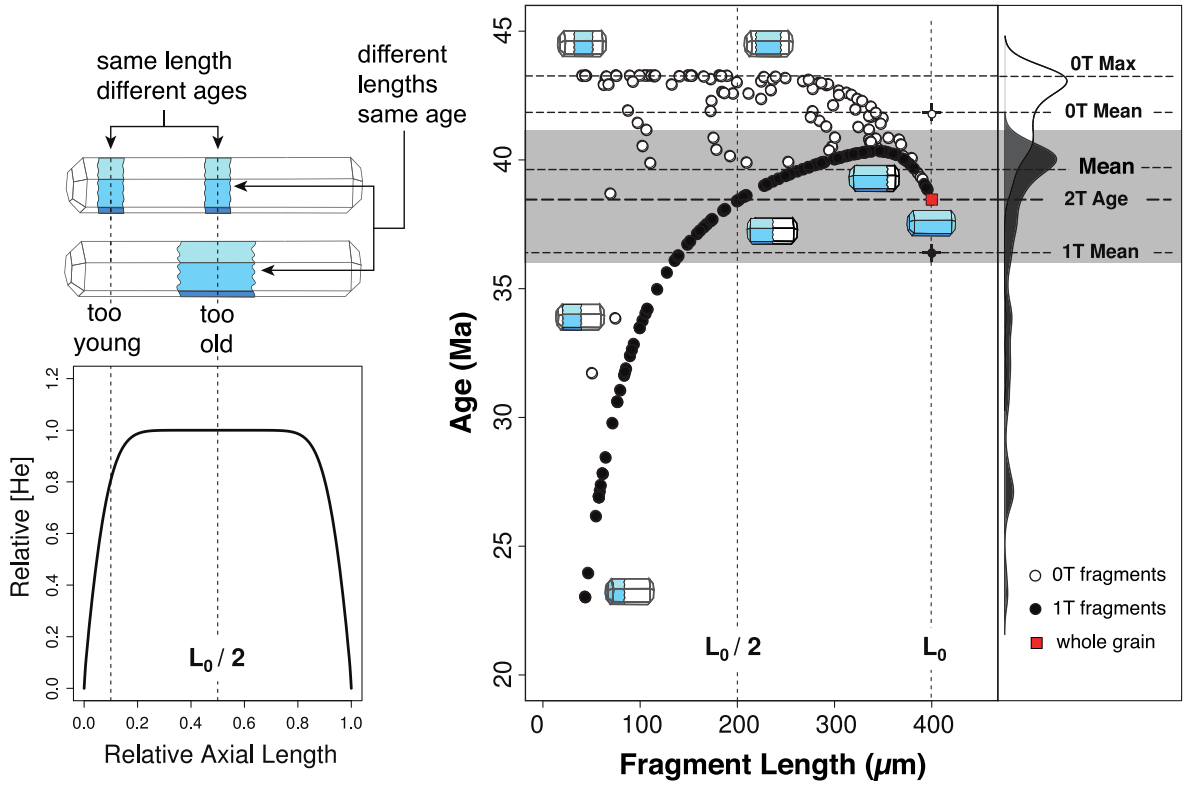

Fig. 5. An annotated age dispersion fragment distribution (ADFD) plot for the WOLF-5 thermal history (symbols as for Fig. 4). Plot of fragment age versus fragment length for sets of fragments with one termination (1T fragments, white circles) and no terminations (0T fragments, filled circles) randomly cut from the same initial grain (L_0 is the initial whole grain length, 400 μm, and R_0 is the grain cylindrical radius, 75 μm and a nominal [U] and [Th] concentration of 20 ppm) for the WOLF-5 thermal history. Note how the age-length trajectory defined by the 1T fragment ages (filled circles) on the ADFD plot mimics the shape of the axial helium diffusion profile for the whole grain (inset left). The relative sizes of fragments and their location relative to the centre of the whole grain are shown schematically by the small cartoon grains. Note that 0T fragments can have the same length but yield different ages, or yield the same age and have different lengths, depending on their position relative to the ends of the whole grain (inset, left). The maximum and mean ages for different groups of fragments are shown by the horizontal dashed lines; 0T Max age 43.3 Ma, 0T Mean age 41.9 Ma, Combined Mean age (1T and 0T fragments) 39.7 Ma, 2T Age (i.e. whole grain) 38.5 Ma and 1T Mean age 37.5 Ma. The horizontal grey band indicates a typical analytical uncertainty of 7% on the whole grain age (38.5 ± 2.6 Ma). The detailed behaviour of both fragment sets is discussed in the text. (For interpretation of the references to colour in this figure legend, the reader is referred to the web version of this article.)

and similar plots for the WOLF-1-4 histories are included in the Electronic annex (Figs. EA-1 to EA-4). These plots clearly illustrate how the complexity of the age dispersion pattern increases with an increasing number of free parameters, and emphasises why 'clean' simple ADFD plots like those shown in Figs. 4 and 5 should not be expected for real samples. This experiment demonstrates several other useful observations about the behaviour of the dispersion pattern. Firstly, it shows that the maximum amount of dispersion for a set of fragments with constant radius is a function of the initial grain cylindrical radius, not its aspect ratio. Secondly, the absolute amount of dispersion expected increases with increasing cylindrical radius, and lastly that the amount of dispersion arising from fragmentation (c. 7% to 60%) is of a similar magnitude to that caused by differences in absolute grain size (R^* 56–164 μm). Summary statistics for the dispersion observed for all five histories are listed in Table EA-1 and detailed fragment lists for all models are included in the Electronic annex.

3.2.3. Including the effects of radiation damage accumulation and annealing

To examine the more realistic situation where there would be a range of initial grains with different absolute grain sizes and geometries as well as differences in eU content we ran some experiments for the five WOLF reference histories where we allowed both grain size and eU to vary. The first experiment included four systematic sets of cylindrical grains whose spherical equivalent radii increased systematically from 50 to 150 μm, with each set of grains having a constant eU content of 5, 20, 40 and 100 ppm, respectively. From these systematic sets of whole grains we then generated random sets of 1T and 0T fragments. The result of this experiment for the WOLF-5 history is summarised in Fig. 7a and the results for the WOLF-1, 2, 3 and 4 histories are illustrated in Figs. EA-5 to EA-8.

To illustrate the combined effects of the three natural sources of dispersion and how they interact we have plotted the model whole grain and fragment ages on standard age

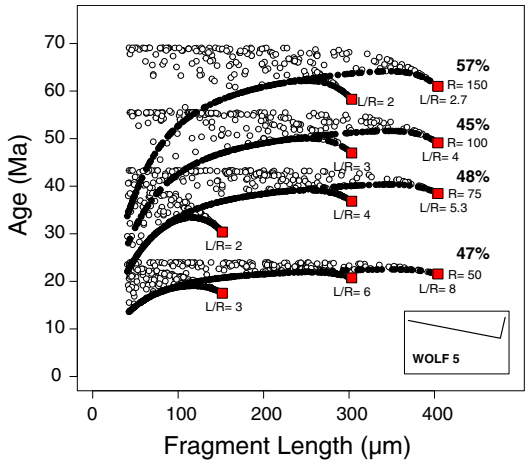

Fig. 6. Age dispersion fragment distribution (ADFD) plot illustrating dispersion patterns for a systematic set of 100 single terminated (1T) fragments (white circles) and 100 fragments with no terminations (0T) fragments (filled circles) derived from a small range of whole grains (red squares) with different lengths, L (125, 300 and 400 μm), radii, R (50, 75, 100, and 150 μm) and aspect ratios (L/R from 2 to 8 and a nominal [U] and [Th] concentration of 20 ppm). The model shown here is for the WOLF-5 thermal history (inset, bottom right). Detailed fragment lists and similar plots for the other WOLF histories are provided in the Electronic Annex and in Figs. EA-1 to EA-4. Note that the maximum amount of dispersion (shown as % for each grain radius) is a function of grain radius and not length, and that the absolute amount of dispersion increases with increasing radius. (For interpretation of the references to colour in this figure legend, the reader is referred to the web version of this article.)

versus R^* and age versus eU plots in Fig. 7a and b, respectively. If we look first at Fig. 7a which plots the grain (either fragment or whole grain) age versus spherical equivalent radius, R^*, it is clear that including variable eU and the effect of radiation damage into the model causes a very large amount of dispersion with ages ranging from circa 5 Ma to over 80 Ma for grains with the same R^* value. This effect is sensitive to the thermal history of course, and the amount of dispersion diminishes systematically with decreasing amounts of diffusional helium loss, as illustrated by the dispersion patterns obtained for the WOLF-1–4 thermal histories (see Figs. EA-5 to EA-8).

This relationship between eU and R^* clearly shows why it is quite possible, likely even, to have very small grains yielding much older ages than very large grains so long as the small grains have significantly higher eU contents than the larger grains. For example, in Fig. 7a there are whole grains with ages of c. 70 Ma for R^* of 50 μm and eU of 100 ppm whereas much larger grains with R^* of 120 μm yield ages of only c. 10 Ma if they have an eU of c. 5 ppm. It is also possible, but less likely, to have grains with higher eU yielding younger ages than grains with lower eU, so long as the grains with higher eU are small enough (see Fig. 7c). The effects of eU and grain size act in opposing directions and so when combined they can lead to complex grain dispersion patterns.

To further emphasise this complex interaction between these competing controls on dispersion we ran another experiment where we simply generated a random set of 1T and 0T fragments from a random selection of grains drawn from the sets of whole grains shown in Fig. 7a. This experiment would closely represent a real sample with a fairly large, but not unrealistic, range of eU values. The results for this experiment are shown in Fig. 7b and c in the form of standard age versus R^* and age versus eU plots, respectively. The equivalent results for the WOLF-1–4 histories are illustrated in Figs. EA-5 to EA-8. The age versus R^* plot for the random fragment experiment (Fig. 7b) illustrates a much more complex pattern of dispersion, clearly showing the large-grain with young-age (e.g. $R^* = 120$ μm, eU = 6 ppm, AHe age = 18 Ma) versus small-grain with old-age ($R^* = 65$ μm, eU = 40 ppm, AHe age = 55 Ma) problem caused by the competing effect of R^* and eU combined with additional corruption caused by fragmentation.

This experiment nicely illustrates the dominance of the radiation damage effect which manages to retain the generally positive age versus eU pattern, with the variance being caused by the combined effects of both grain size and fragmentation (Fig. 7c). Note that some of the additional variance arises because the R^* value for fragments actually underestimates the effective radius/size of the grains thus corrupting any real relationship between size and age. Summary statistics for the dispersion patterns generated in this experiment are listed in Table EA-2 for all of the WOLF-1-5 histories.

The age versus eU plots for the random experiments summarised in Fig. 7c and Figs. EA-5c to EA-8c also illustrate that the radiation damage effect reaches a saturation point, such that above a certain eU value (unique for each thermal history) the ages for grains with eU values greater than this threshold do not increase further. For example, for the WOLF-5 history this threshold eU value is reached at approximately 50 ppm (Fig. 7c). This phenomenon explains why it is sometimes possible to observe only very weak or no correlation between AHe age and eU values, even for complex thermal histories, if the eU values for all grains are greater than this saturation value. The detailed behaviour of this phenomenon, and its dependence on the thermal history in particular, is related to the specific parameterisation and calibration of the particular radiation damage and annealing model used (here we use the RDAAM model of Flowers et al., 2009) and further analysis of this phenomenon seems worth while, but is beyond the scope of this paper.

3.3. Competing dispersion effects and decoupling caused by fragmentation

It is clear from the analysis above that the natural dispersion effects arising from differences in grain size and eU act independently. On 2D plots of age versus R^* and age versus eU these causes of dispersion effectively compete with each other by acting in orthogonal directions on these plots and adding apparent 'noise' to the expected correlations between age and either R^* or eU, respectively (Fig. 8). Fragmentation clearly acts to decouple the relationships between grain age, R^* and eU even further because fragmentation acts to either decrease or increase the fragment age relative to the whole

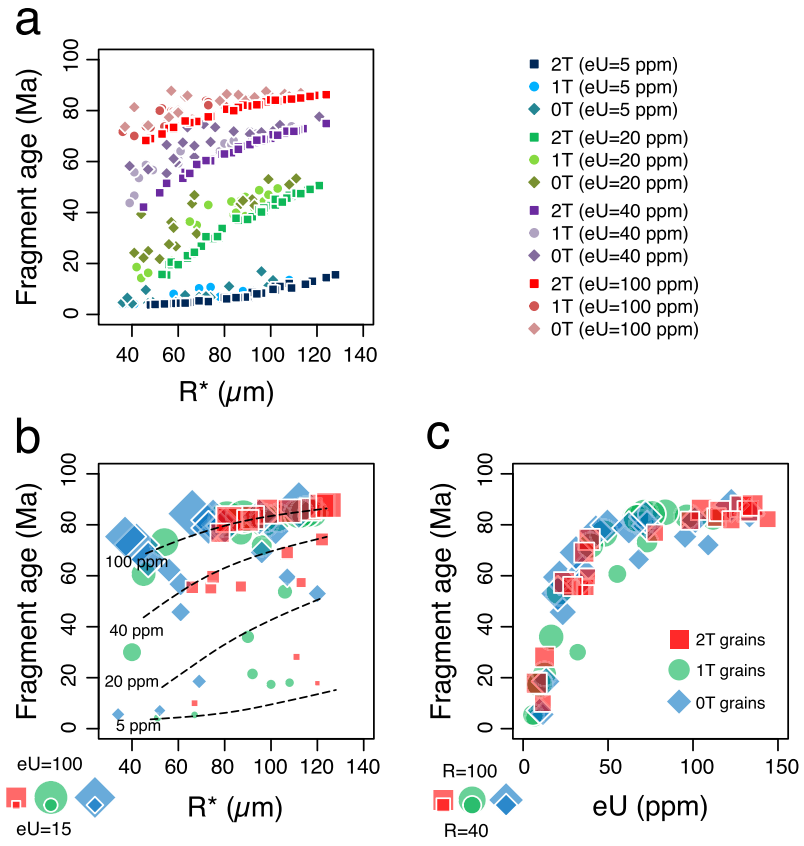

Fig. 7. Model of dispersion patterns including all three causes of natural dispersion, namely fragmentation, grain size and radiation damage effects for the WOLF-5 thermal history. (a) Plot showing grain age versus spherical equivalent radius, R^*, for sets of whole grains (filled squares) for a range of eU contents (5, 20, 40 and 100 ppm) and for sets of fragments (1T fragments are filled circles and 0T fragments are filled diamonds) derived from these whole grains. On this diagram the fragment ages always plot to the left (lower R^* values) of the whole grain trajectories but can have either older or younger ages than their respective whole grain age. (b) Plot of grain age versus R^* for a set of fragments with random sizes and random eU values derived from the array of whole grains shown in Fig. 7a. The shape of the symbols indicates the fragment type as in (a), and the size of the symbol indicates the eU concentration of each grain. The dashed black lines are contours for equivalent eU. (c) Plot of grain age versus eU for the same set of fragments shown in Fig. 7b. The shape of the symbols indicates the fragment type as in (b), and the size of the symbol indicates the cylindrical grain radius of each grain. Note the saturation of the radiation damage effect for eU values greater than 50 ppm. Detailed fragment lists for all models and similar plots for the other WOLF histories are provided in the Electronic Annex and in Figs. EA-5 to EA-8.

grain age and so 'pulls' the points off the whole grain trajectories on these plots, moving them to the upper left or lower left on an age versus R^* plot (Fig. 8a) or vertically up or down on an age versus eU plot (Fig. 8b). An excellent example of this decoupling phenomenon expressed for whole grain analyses is illustrated and discussed in detail by Flowers and Kelley (2011) for a set of closely related samples from basement rocks in northeastern Kansas.

4. IMPLICATIONS FOR (U–TH)/HE THERMOCHRONOMETRY

As a framework for discussing the implications of these model findings for practical applications of the (U–Th)/He thermochronometry we will examine the dispersion patterns demonstrated by some natural data and compare these with the patterns generated above using our fragmentation model. There are two primary implications we believe. The first is simply that including fragmentation into the mix of causes of dispersion, and analysing the interaction of the competing effects, provides a template that makes sense of many observed patterns of dispersion where before there was no apparent pattern to this. The second implication, and by far the most important one, is the recognition that the pattern of dispersion arising from fragmentation contains useful thermal history information because it provides a proxy for the axial diffusion profiles of ^{4}He within the whole grains from which the fragments were derived. We will discuss both these implications in the context of patterns of dispersion that might be observed for a set of different but related samples, i.e. a set of samples collected from a vertical topographic profile and for dispersion behaviour observed for grains from a single sample.

An ideal exemplar data set is documented by Fitzgerald et al. (2006) from the Ferrar Glacier region in the Transantarctic Mountains. In this study two sets of samples were collected from steep vertical topographic profiles on either side of the Ferrar Glacier, one from Cathedral Rocks and

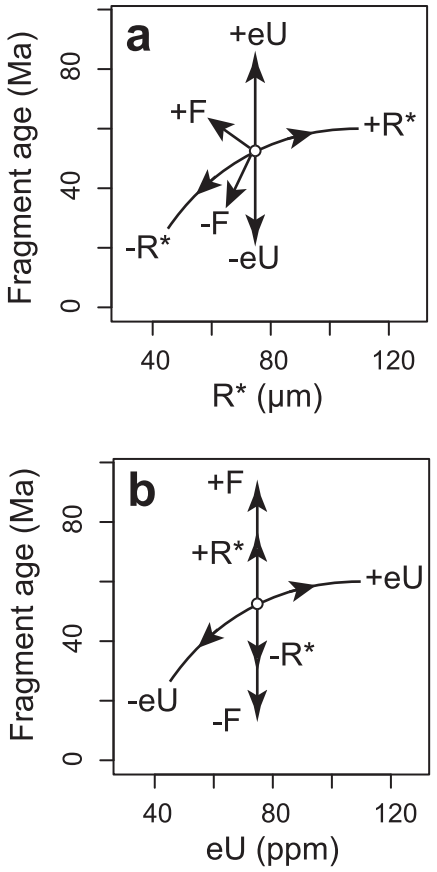

Fig. 8. Cartoon illustrating the relative trajectories and contributions of the competing causes of natural dispersion within the 2 D spaces of (a) grain age versus R^* and (b) grain age versus eU. These competing effects act together to distort and corrupt any correlations between age and R^* and, to a lesser extent eU, and fragmentation (±F) adds additional variance by decoupling the expected patterns further. For any thermal history; +eU (higher effective U concentration) makes an age older whereas eU (lower effective U concentration) makes it younger, while larger grains (+R) are older and smaller grains (−R) are younger, and larger fragments (+F) are typically older whereas smaller fragments (−F) are younger (but all fragments have are clearly smaller than the whole grain, and have smaller R^* values.

one from Peak 1880 in the Kukri Hills. A suite of single grain AHe ages followed collection of a complementary set of apatite fission track data (AFT) for all samples. The AHe ages represent a mixture of whole grains (2T) and 1T and 0T fragments in this case. The advantage of this set of data in the context of this study is that Fitzgerald et al. (2006) were able to constrain the cooling rate using the AFT data and use that to establish that AHe single grain age dispersion varied with cooling rate, with dispersion being greater when the cooling rate was slower, or samples resided within the helium partial retension zone (PRZ) for significant periods of time. Also, the two vertical profiles had similar cooling/exhumation histories, but with a fault offset of c. 370 m across the intervening glacial valley. Peak 1880 was downthrown c. 370 m relative to Cathedral Rocks, but is also slightly closer to the faulted Transantarctic Mountain front and active West Antarctic rift. The timing of key cooling events was the same for both profiles, slow cooling in the Cretaceous and early Eocene was followed by faster cooling in the Eocene, beginning at c. 50–45 Ma. So all samples from the composite profile would have experienced the same episodes of cooling or heating, but with samples at higher elevations (shallower crustal level) experiencing lower maximum paleotemperatures than those at lower elevations (deeper crustal level), but with the timing of key cooling events being the same for all samples. These data and the very systematic pattern of AHe age dispersion with increasing sample elevation are illustrated using the reconstructed (both profiles combined after fault offset is restored) composite elevations in Fig. EA-9. In the following sections we will discuss the observed pattern of dispersion between different samples from the profile, followed by discussion of the intra sample single grain dispersion behaviour.

4.1. Dispersion patterns observed between different, but related samples

Although the number of single grain AHe ages from each of the Ferrar Glacier samples is relatively small (typically between 3 and 6) there is a sufficiently large number of closely spaced samples to capture what appears to be a very systematic pattern of dispersion between the different samples making up the profile (Fig. EA-9). The lower samples, below elevations of c. 450 m, all display uniformly smaller amounts of dispersion whereas samples at higher elevations consistently display much larger amounts of dispersion of the AHe ages. Interestingly, the mean AHe age for each elevation forms a systematic pattern decreasing with elevation down to circa 450 m and then remains essentially constant at c. 30 Myr below this elevation. This behaviour in the inter sample dispersion and in the pattern of progressively increasing dispersion above a threshold height is exactly what would be expected for the thermal history style envisaged by Fitzgerald et al. (2006), and was what this study actually observed in the variation of single grain ages. In this case the lowest samples with minimal dispersion are interpreted to have cooled quickly through the helium partial retention zone (PRZ) during the Eocene event (at c. 40 Ma) with the higher samples (above c. 450 m) residing within the PRZ prior to rapid cooling in the Eocene.

To analyse this pattern of dispersion behaviour in a quantitative manner we have constructed a hypothetical vertical profile section, scaled to be similar to that for the Ferrar Glacier data (i.e. similar grain size and eU range), and using a simple two stage thermal history comprising isothermal heating between 90 and 40 Ma followed by rapid cooling to surface temperatures by 39 Ma (see Fig. EA-10 and Table EA-3), similar to that envisaged by Fitzgerald et al. (2006). We emphasise though that this model is not an attempt to actually model the thermal history for these data in a formal manner, but rather to illustrate how the pattern of dispersion can be understood in detail, and to emphasise how information about the thermal history is recorded by the AHe age dispersion pattern itself. For example, the rate of cooling estimated by Fitzgerald et al. (2006) after c. 40 Ma was found to be more rapid than

the rate of cooling before c. 40 Ma when samples cooled very slowly through a PRZ, although in geologic terms the post 40 Ma cooling is still very slow. For the sake of this study and to understand patterns of dispersion we model cooling after c. 40 Ma as very rapid. For this experiment we generated several sets of fragments for a range of model samples (each at a different elevation) separating out the competing effects of fragmentation, grain size, and the radiation damage effect and a final set of fragments including all these effects together. In all cases the fragment lists were randomly generated and these are provided in the Electronic annex and summary statistics of the dispersion patterns for each elevation are listed in Table EA-4. The results of this experiment are illustrated and summarised in Fig. 9 and are also shown relative to the observed data in Fig. EA-9 for comparison. The systematic change in the pattern of AHe age dispersion with sample elevation is analogous to the systematic changes that occur in the apatite fission track (AFT) age and track length distributions with elevation (the observed apatite fission track ages and track length distributions for four samples are shown on Fig. EA-9 for reference).

The similarity in the behaviour and pattern of AHe age dispersion with increasing elevation shown in Fig. 9 is strikingly similar to that displayed by the Ferrar Glacier data, and if anything, it emphasises that the real data have underestimated the true amount of dispersion, probably because there are relatively few single grain data.

4.2. Dispersion patterns observed within single samples

As a further test of the dispersion model, we randomly selected 15 grains (including 5 each of 2T, 1T and 0T grains) from those generated for model elevations of 1600 m, 800 m and 0 m, and examined the pattern of dispersion as seen on standard age R^* and eU plots as well as our ADFD plots (Fig. 10). These models display very systematic patterns of dispersion for grains from the individual samples for different elevations. The model sample at 0 m elevation cooled rapidly through the PRZ to near surface temperatures (25–18 °C) from a maximum paleotemperature of 85 °C (see Fig. EA-10) and consequently displays minimal dispersion. The two higher samples, on the other hand, resided within the PRZ for a significant period of time between 90 and 40 Ma prior to rapid cooling to surface temperatures (0–7 °C) and consequently display significant, and critically, quite complex patterns of dispersion as expected.

To compare these model patterns of intra sample dispersion with the observed data we selected two sets of the Ferrar Glacier data; one to represent a sample that cooled quickly through the PRZ and the other to represent a sample that resided within the PRZ prior to cooling. The pattern of dispersion for the two groups of samples from the Ferrar Glacier profile are shown on standard age versus R^* and age versus eU plots in Fig. 11 together with the model grain ages for model elevations of 0 m and 600 m, respectively. For the higher set of samples (model elevations between 577 and 751 m), which are interpreted to have resided within the PRZ prior to rapid cooling in the Eocene, there are no obvious correlations between age and either R^* or eU despite there being a reasonably large range in single grain ages (between 50 and 30 Ma). This behaviour is matched reasonably well by the model dispersion pattern for the 600 m sample (Fig. 11a and b). On the other hand, for the lower set of samples (model elevations between −71 and 361 m) which are interpreted to have cooled quickly through the PRZ, (Fig. 11c and d), all grains have quite similar ages apart from one old grain, despite having a range of grain sizes and eU contents. The model dispersion pattern for the 0 m elevation sample, which represents the equivalent position in the profile, matches the observed dispersion pattern quite well (Fig. 11c and d). This difference in intra sample dispersion behaviour is exactly what is expected for different sets of samples that have all cooled at the same time but from different maximum palaeotemperatures. The first set having experienced significant thermal diffusion (the higher samples) during residence within the PRZ, and the second a set that cooled quickly through the PRZ and so have not experienced significant diffusional loss of helium (the lower samples).

We suggest that a key implication of this analysis of dispersion, and emphasised particularly with the Ferrar Glacier experiment, supports previous work (Fitzgerald et al., 2006; Flowers, 2009; Ault et al., 2009; Flowers and Kelley, 2011) that indicates it is unreasonable to expect a small number of single grain AHe ages (say 3–5 grains) to (a) reproduce, and (b) to characterise the full range of true age dispersion for samples that have experienced protracted, non-monotonic thermal histories. This could only be possible if all the grains were of a very similar true size, were whole crystals and had very similar eU contents. But, the most important implication, from a thermochronometry point of view at least, is that it is the pattern of dispersion that contains the information about the thermal history, and so if sampling strategies and analytical protocols are designed to minimise this dispersion they will be effectively minimising the thermal history information in the data. A single, discrete, AHe age for a sample could indicate the simplest possible thermal history, i.e. that the sample cooled rapidly at approximately the time indicated by the age. Without independent information about the distribution of helium within the grains though this interpretation is ambiguous.

5. DISCUSSION AND CONCLUSION

Dispersion of individual grain AHe ages obtained for a single rock sample is caused by a mixture of natural, inherent effects related to the normal response of an otherwise ideal, well behaved system and extraneous imposed effects that add unwanted noise to the data. In some circumstances the magnitude of the inherent, natural dispersion is significantly larger than that caused by unwanted extraneous effects (typically of order 5–15%) other than for very rare or unusual circumstances. For samples that have experienced significant (i.e. $> 20\%$) helium loss due to thermal diffusion this useful dispersion is typically of the order of 50–100%. The three known useful causes of age dispersion are differences in grain size, differential radiation damage accumulation and annealing caused by differences in eU content and the fragmentation effect described in this paper.

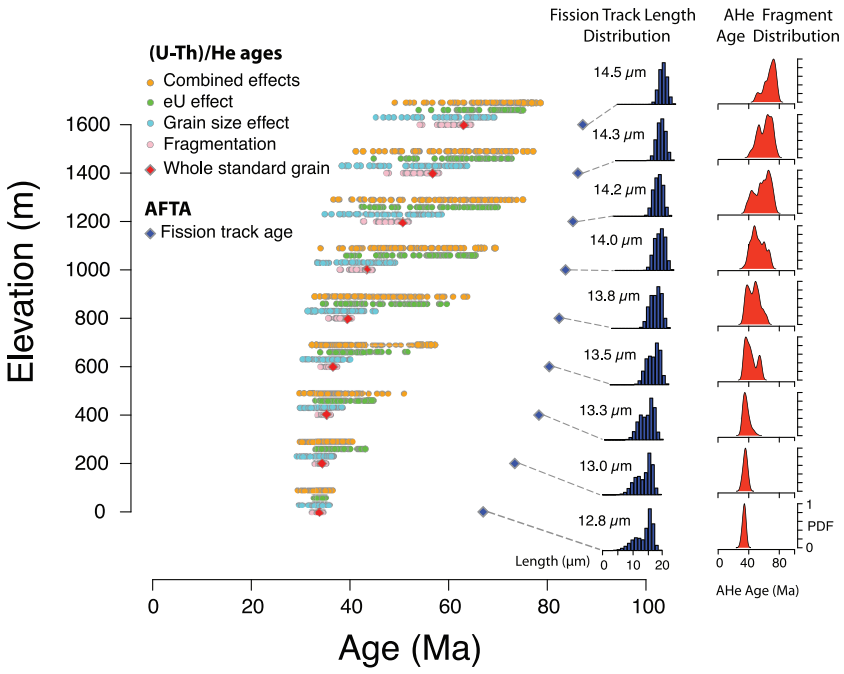

Fig. 9. Results of an experiment designed to illustrate the relative contribution of the causes of natural dispersion and the pattern of dispersion expected for a set of samples similar to that from the Ferrar Glacier profile samples (see comparison in Fig. EA-9 and statistics summary in Table EA-4). The thermal history used to generate the model data involved isothermal heating between 90 and 40 Ma followed by very rapid cooling to surface temperatures at 39 Ma (see Fig. EA-10, Table EA-3). Grains sizes ($^{*}R$) range between 32 and 74 μm and eU concentrations between 15 and 100 ppm. All samples cooled at 40 Ma with successively lower elevation samples having cooled from progressively higher maximum paleotemperatures. Model AHe fragment ages (filled circles) and model AFT ages (filled blue diamonds) are shown plotted against model sample elevation. Note that the amount of dispersion is least at the bottom and increases systematically with increasing elevation until c. 1300 m. This reflects the increased degree of 'rounding' on the helium diffusion profiles for grains from higher elevations caused by the higher proportion of 'old' helium relative to 'young' helium (i.e. helium accumulated after rapid cooling) preserved in the grains. The lowest sample has the least dispersion because it contains virtually no 'old' helium and the diffusion profiles in all the grains are effectively uniform and 'flat'. The total dispersion begins to decrease with increasing elevation above c. 1300 m because the degree of helium loss during the isothermal heating phase begins to decrease. Model fission track length distributions (in blue) and fragment age probability distribution functions for the 'combined effects' model of dispersion (in red) are illustrated on the right of the figure to emphasise that the detailed anatomy of the pattern of AHe age dispersion in each sample is analogous to the distribution of fission track lengths, both reflecting the sample's thermal history through the partial annealing zone (PAZ) or partial retention zone (PRZ), respectively. In this synthetic model the lowest samples experienced maximum palaeotemperatures of c. 85 °C (i.e. within the fission track PAZ), and so the track length distributions indicate significant annealing (presence of shortened tracks). Complete fragment lists for all of the model samples, including predicted fission track parameters, are provided in the Electronic Annex. (For interpretation of the references to colour in this figure legend, the reader is referred to the web version of this article.)

Because these three causes of natural of dispersion are inherent to the system it is unreasonable to expect single grain ages performed on grains of different size and eU content to reproduce for any sample that has not experienced rapid, monotonic cooling through the partial retention zone.

The analysis of dispersion presented here clearly shows that the amount of dispersion arising from the routine analysis of broken apatite crystals (c. 7–60%) is of a similar order of magnitude to that caused by grain size variation alone for reasonable ranges in grain size (i.e. 50–150 μm). Dispersion arising solely from radiation damage effects caused by differences in eU content can be very large, and could exceed 100% for some thermal histories and reasonable ranges of eU (i.e. 5–100 ppm). The relative contributions from each source of dispersion for any data set is ultimately controlled by the thermal history of the sample, the range of eU, range of initial grain size and the morphology of grains and fragments selected for analysis. In addition to adding significantly to the total amount of dispersion observed in real data, the fragmentation effect also acts to decouple and corrupt expected correlations between grain age and grain size and eU. Furthermore, if the spherical equivalent radius of a fragment is used as a measure of the diffusion domain, either to plot age versus grain size plots or as input to thermal history models, then the effective size of the grain will be underestimated, adding additional unwanted variance to correlations and/or leading to erroneous thermal histories being derived.

In general, when applying the (U–Th)/He thermochronometer, a wide range of single grain AHe ages well outside the standard analytical error should be the expected norm, even with complete absence of any extraneous sources of dispersion. The range of this natural dispersion is typically an order of magnitude larger than the standard deviation

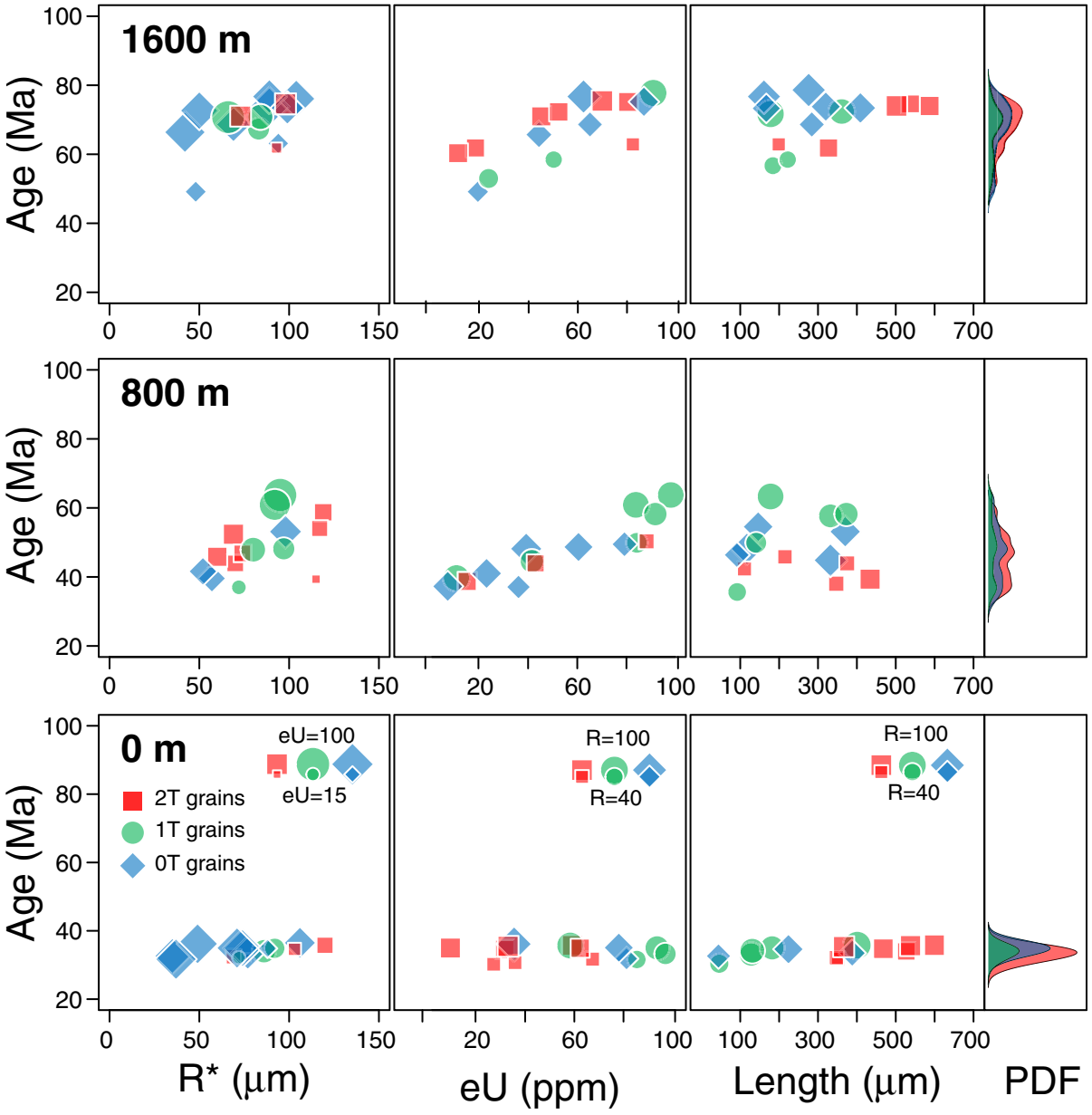

Fig. 10. Intra-sample model dispersion patterns for samples from the Ferrar Glacier profile shown in Fig. 9. A selection of 15 random fragment ages drawn for three model samples from 1600 m, 800 m and 0 m are shown on standard grain age versus R^* (symbol size indicates eU concentration), grain age versus eU and our ADFD plots (where symbol size indicates cylindirical grain radius). The shape and colour of the symbols indicates fragment type as in previous figures (see legend for 0 m elevation sample). The two samples from 800 m and 1600 m represent samples that have experienced protracted thermal histories with significant time spent within the PRZ and consequently show complex dispersion patterns. The lowest sample from 0 m elevation has cooled quickly through the PRZ and so all grains have similar ages. Simple probability distribution curves (PDF) for the fragment ages for each model sample are shown on the right of the figure to emphasise that the structure of the AHe age dispersion for each sample reflects its thermal history. Note that the two higher samples have complex and different PDF curves (complex histories) while the lowest sample has a simple PDF curve (simple history).

for a set of grains for samples with protracted thermal histories. If standard grain screening protocols are used to select grains free of inclusions, and where feasible, assessments are made of the typical spatial distributions of [U] and [Th] within the grains either by LA-ICPMS (e.g. Farley et al., 2011; Ault and Flowers, 2012), or simply by carrying out fission track analyses first, then this age dispersion will most likely contain useful, accessible thermal history information about the sample. Grain selection strategies and analytical protocols that attempt to minimise the age dispersion within a sample (e.g. picking similar sized grains, abrading the outer rims or eliminating outliers) will

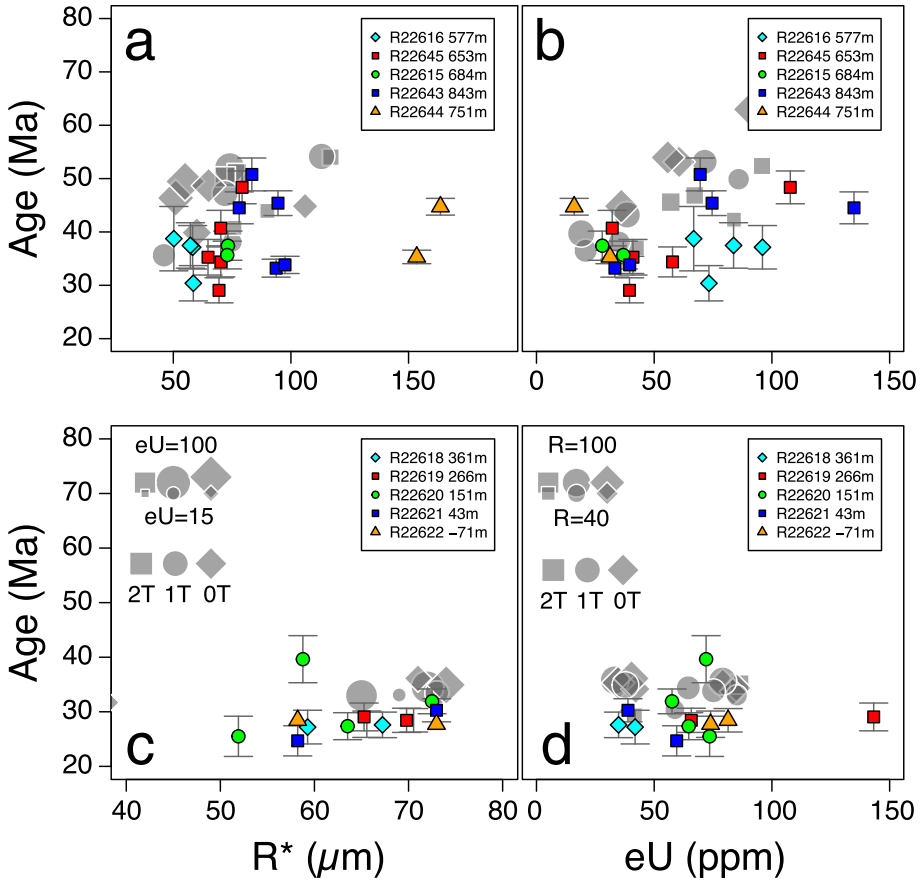

Fig. 11. Comparison of observed and model intra-sample dispersion patterns for selected samples from the Ferrar Glacier profile data of Fitzgerald et al. (2006). (a) Standard grain age versus R^* and (b) age versus eU diagrams for single grain ages from samples with model elevations between 577 and 751 m. The shapes and colours of coloured symbols indicate the sample number (see legend). The larger, grey symbols indicate the model fragment ages for the 600 m sample shown in Fig. 9. The shape of the grey symbols indicates fragment type and the size of the grey symbols indicates either eU or grain radius, respectively (see legends). (c) Standard grain age versus R^* and (d) age versus eU diagrams for single grain ages from samples with model elevations between 361 and −7 m. The larger, grey symbols indicate the model fragment ages for the 0 m sample shown in Fig. 9 with symbology as for (a) and (b) above. (For interpretation of the references to colour in this figure legend, the reader is referred to the web version of this article.)

effectively also minimise the amount of usable thermal history information in the resulting data. Furthermore, where a sample displays significant natural dispersion it is unclear how a single age for that sample can be compared with the age or ages obtained using a different thermochronometer or geochronometer. It is probably best in this circumstance to report the full range of grain ages obtained along with appropriate summary statistics without inferring that the sample is characterised by any single AHe age. It remains moot though whether, and how, a meaningful correction for alpha ejection could be made for this purpose to ages for samples that have experienced severe diffusional loss of ^{4}He. In these circumstances it is likely better to derive thermal history constraints for the sample using the raw, uncorrected, AHe ages and to compare the timing and style of history obtained with that indicated by other thermochronometers.

In practice, if the primary focus of a study is to extract the thermal history information from (U–Th)/He analyses we suggest that field sampling and analytical strategies, such as that used by Ault et al. (2009) and Flowers (2009), which aim to maximise the natural dispersion of ages are desirable, and that circa 20–30 grains from each sample should be analysed. This may well require analysing more grains from less samples than is currently the norm, and should ideally include picking very short and very long as well as wide and thin (within reason, i.e. keep $R > 40$ μm) fragments as well as any whole grains that exist, and noting carefully how many terminations each fragment or grain has. In some cases, where only whole grains of a similar dimension are available, the thermal history modelling process might be enhanced by carefully breaking the whole crystals to create fragments. This approach needs to be empirically tested though. Additionally, thermal history inversion procedures should avoid representing fragments using the spherical equivalent radius based on the fragment dimensions, and should ideally be adapted to enable broken crystals to be modelled explicitly as fragments of larger crystals.

Some specific conclusions about interpreting a range of AHe ages obtained from, or including, analyses performed on broken crystals from a single sample are;

- The youngest age, on its own, is unlikely to represent a useful or meaningful age for the sample.
- Fragments retaining a single termination (1T grains) can yield ages which are either older or younger than the whole grain age.
- Fragments with no terminations (0T grains) are most likely to yield ages that are older than the whole grain age, and are also the most likely to produce replicate analyses, but these replicates would not record a directly meaningful age or the whole grain age. 0T fragments of very different length (size) can yield identical ages, and 0T fragments with identical length (size) can yield significantly different ages.
- For a sufficiently large number of analyses (maybe > 20?) the mean fragment age may well approximate a useful measure of the AHe age of a sample for qualitative comparative purposes only, effectively representing the 'average age for the average grain analysed'.
- When plotting standard age versus grain size plots it is probably better to use the actual grain half width or cylindrical radius than to use the spherical equivalent radius because it provides a better estimate of the dominant diffusion dimension for fragments. In all cases though, interpreting patterns of dispersion using standard age versus grain size and/or age versus eU plots should exercise caution because of the competing effects of grain size and eU and the additional decoupling effect of fragmentation. In effect, the lack of a positive correlation between age and grain size or age and eU on these plots does not mean that there is no correlation; it is likely simply obscured by the complex interplay of all three sources of natural dispersion plus any additional noise.

The most important implication of this analysis of dispersion, we believe, is that it implies that rather than producing unwanted 'noise' the pattern of dispersion caused by fragmentation actually contains useful, accessible information about a sample's thermal history. This information can be practically used to help constrain thermal histories, and most importantly, to discriminate between sample histories that yield similar standard grain AHe ages in a manner similar to the $^4He/^3He$ technique. A new inversion approach to thermal history modelling incorporating this idea is described in detail in a companion paper (Beucher et al., 2013 this volume).

And finally, although this study has focused on the implications for the (U–Th)/He thermochronometer the analysis of fragmentation and thermal diffusion and many of the specific conclusions are applicable to other systems where the diffusion domain size is approximated by the physical grain dimensions, such as the apatite, titanite and rutile U–Pb thermochronometers for example (Chamberlain and Bowring, 2001; Schoene and Bowring, 2007; Blackburn et al., 2011, 2012) or the Sm–Nd and Lu–Hf decay systems in garnet (Ganguly and Tirone, 1999).

ACKNOWLEDGEMENTS

This work has benefited from numerous conversations and discussions with colleagues and graduate students and we acknowledge this and particularly the generous insight into causes and patterns of dispersion shared with us by Kerry Gallagher, Rich Ketcham, Sean Willett, Ryan McKeon, Charles Kasanzu and Mark Wildman. Comprehensive and constructive reviews from Alexis Ault, Ryan McKeon and Pieter Vermeesch are gratefully acknowledged. This research was supported by NERC Grants NE/J013242/1 and NE/H008276/1 held at GU and NE/H008454/1 held at SUERC. Fitzgerald acknowledges support from National Science Foundation Grant OPP-0002824. Samples from the Ferrar Glacier region of the Tranantarctic Mountains were originally collected as part of fieldwork supported by the Antarctic Research Centre of Victoria University of Wellington.

APPENDIX A. SUPPLEMENTARY DATA

Supplementary data associated with this article can be found, in the online version, at http://dx.doi.org/10.1016/j.gca.2013.05.041.

REFERENCES

Ault A. K. and Flowers R. M. (2012) Is apatite U–Th zonation information necessary for accurate interpretation of apatite (U–Th)/He thermochronometry data? *Geochim. Cosmochim. Acta* **79**, 60–78.

Ault A. K., Flowers R. M. and Bowring S. A. (2009) Phanerozoic burial and unroofing history of the western slave craton and wopmay orogen from apatite (U–Th)/he thermochronometry. *Earth Planet. Sci. Lett.* **284**(1), 1–11.

Beucher R., Brown R., Roper S., Persano C., Stuart F. and Fitzgerald P. (2013) Natural age dispersion arising from the analysis of broken crystals. Part II. Practical application to apatite (U–Th)/He thermochronometry.

Blackburn T., Bowring S. A., Schoene B., Mahan K. and Dudas F. (2011) U–Pb thermochronology: creating a temporal record of lithosphere thermal evolution. *Contrib. Mineral. Petrol.* **162**(3), 479–500.

Blackburn T. J., Bowring S. A., Perron J. T., Mahan K. H., Dudas F. O. and Barnhart K. R. (2012) An exhumation history of continents over billion-year time scales. *Science (New York, NY)* **335**(6064), 73–76.

Carlson W. D., Donelick R. A. and Ketcham R. A. (1999) Variability of apatite fission-track annealing kinetics: I. Experimental results. *Am. Mineral.* **84**(9), 1213–1223.

Chamberlain K. R. and Bowring S. A. (2001) Apatite-feldspar U–Pb thermochronometer: a reliable, mid-range (450 °C), diffusion-controlled system. *Chem. Geol.* **172**(1–2), 173–200.

Cherniak D., Watson E. and Thomas J. (2009) Diffusion of helium in zircon and apatite. *Chem. Geol.* **268**(1–2), 155–166.

Ehlers T. A., Chaudhri T., Kumar S., Fuller C. W., Willett S. D., Ketcham R. A. and Fu F. Q. (2005) Computational tools for low-temperature thermochronometer interpretation. *Rev. Mineral. Geochem.* **1**(58), 589–622.

Farley K., Shuster D. and Ketcham R. (2011) U and Th zonation in apatite observed by laser ablation ICPMS, and implications for the (U–Th)/He system. *Geochim. Cosmochim. Acta* **75**(16), 4515–4530.

Farley K. A. (2000) Helium diffusion from apatite: general behavior as illustrated by Durango fluorapatite. *J. Geophys. Res.* **105**(B2), 2903.

Farley K. A. (2002) (U–Th)/He dating: techniques, calibrations, and applications. *Rev. Mineral. Geochem.* **47**(1), 819–844.

Farley K. A., Shuster D. L., Watson E. B., Wanser K. H. and Balco G. (2010) Numerical investigations of apatite ^{4}He/^{3}He thermochronometry. *Geochem. Geophys. Geosyst.* **11**(10).

Farley K. A. and Stockli D. F. (2002) (U–Th)/He dating of phosphates: apatite, monazite, and xenotime. *Rev. Mineral. Geochem.* **15**, 559–578.

Farley K. A., Wolf R. A. and Silver L. T. (1996) The effects of long alpha-stopping distances on (U–Th)/He ages. *Geochim. Cosmochim. Acta* **60**(21), 4223–4229.

Faure G. and Mensing T. (2005) *Isotopes: Principals and Applications*. Wiley.

Fitzgerald P., Baldwin S., Webb L. and O'Sullivan P. (2006) Interpretation of (U–Th)/He single grain ages from slowly cooled crustal terranes: a case study from the Transantarctic Mountains of southern Victoria Land. *Chem. Geol.* **225**(1–2), 91–120.

Flowers R., Shuster D., Wernicke B. and Farley K. (2007) Radiation damage control on apatite (U–Th)/He dates from the Grand Canyon region, Colorado Plateau. *Geology* **35**(5), 447–450.

Flowers R., Wernicke B. and Farley K. (2008) Unroofing, incision, and uplift history of the southwestern Colorado Plateau from apatite (U–Th)/He thermochronometry. *Geol. Soc. Am. Bull.* **120**(5–6), 571–587.

Flowers R. M. (2009) Exploiting radiation damage control on apatite (U–Th)/He dates in cratonic regions. *Earth Planet. Sci. Lett.* **277**(1), 148–155.

Flowers R. M. and Kelley S. A. (2011) Interpreting data dispersion and inverted dates in apatite (U–Th)/He and fission-track datasets: an example from the US midcontinent. *Geochim. Cosmochim. Acta* **75**(18), 5169–5186.

Flowers R. M., Ketcham R. A., Shuster D. L. and Farley K. A. (2009) Apatite (U–Th)/He thermochronometry using a radiation damage accumulation and annealing model. *Geochim. Cosmochim. Acta* **73**(8), 2347–2365.

Gallagher K., Brown R. and Johnson C. (1998) Fission track analysis and its applications to geological problems. *Ann. Rev. Earth Planet. Sci.* **26**(1), 519–572.

Ganguly J. and Tirone M. (1999) Diffusion closure temperature and age of a mineral with arbitrary extent of diffusion: theoretical formulation and applications. *Earth Planet. Sci. Lett.* **170**(1–2), 131–140.

Gautheron C., Tassan-Got L., Barbarand J. and Pagel M. (2009) Effect of alpha-damage annealing on apatite (U–Th)/He thermochronology. *Chem. Geol.* **266**(3–4), 157–170.

Gautheron C., Tassan-Got L., Ketcham R. A. and Dobson K. J. (2012) Accounting for long alpha-particle stopping distances in (U–Th–Sm)/He geochronology: 3D modeling of diffusion, zoning, implantation, and abrasion. *Geochim. Cosmochim. Acta* **96**, 44–56.

Harrison T. M., Grove M., Lovera O. M. and Zeitler P. K. (2005) Continuous thermal histories from inversion of closure profiles. *Rev. Mineral. Geochem.* **1**(58), 389–409.

House M., Wernicke B., Farley K. and Dumitru T. (1997) Cenozoic thermal evolution of the central Sierra Nevada, California, from (UTh)/He thermochronometry. *Earth Planet. Sci. Lett.* **151**(3–4), 167–179.

Jäger E. and Hunziker J. (1979) *Lectures in Isotope Geology*. Springer-Verlag Edition.

Ketcham R. A., Carter A., Donelick R. A., Barbarand J. and Hurford A. J. (2007) Improved modeling of fission-track annealing in apatite. *Am. Mineral.* **92**(5–6), 799–810.

Ketcham R. A., Gautheron C. and Tassan-Got L. (2011) Accounting for long alpha-particle stopping distances in (U–Th–Sm)/He geochronology: refinement of the baseline case. *Geochim. Cosmochim. Acta* **75**(24), 7779–7791.

Kohn B. P., Lorencak M., Gleadow A. J. W., Kohlmann F., Raza A., Osadetz K. G. and Sorjonen-Ward P. (2009) A reappraisal of low-temperature thermochronology of the eastern Fennoscandia Shield and radiation-enhanced apatite fission-track annealing. *Geol. Soc. Lond. Spec. Publ.* **324**(1), 193–216.

Lippolt H. J., Leitz M., Wernicke R. S. and Hagedorn B. (1994) (Uranium + thorium)/helium dating of apatite: experience with samples from different geochemical environments. *Chem. Geol.* **112**(1–2), 179–191.

Lovera O. M., Grove M. and Harrison T. (2002) Systematic analysis of K-feldspar ^{40}Ar/^{39}Ar step heating results II: relevance of laboratory argon diffusion properties to nature. *Geochim. Cosmochim. Acta* **66**(7), 1237–1255.

McDougall I. and Harrison T. M. (1999) *Geochronology and Thermochronology by the ^{40}Ar/^{39}Ar Method*. OUP, USA.

Meesters A. and Dunai T. (2002a) Solving the production–diffusion equation for finite diffusion domains of various shapes: Part II. Application to cases with α-ejection and nonhomogeneous distribution of the source. *Chem. Geol.* **186**(3–4), 333–344.

Meesters A. and Dunai T. (2002b) Solving the production–diffusion equation for finite diffusion domains of various shapes: Part I. Implications for low-temperature (U–Th)/He thermochronology. *Chem. Geol.* **186**(3–4), 333–344.

Murray K. E., Orme D.A. and Reiners P. W. (2011) Apatite (U–Th)/He date dispersion due to secondary grain boundary phases: an example from the Henry Mountains, Utah. *AGU Fall Meeting Abstracts-1*, 2556.

Reiners P. W. and Brandon M. T. (2006) Using thermochronology to understand orogenic erosion. *Ann. Rev. Earth Planet. Sci.* **34**(1), 419–466.

Reiners P. W., Ehlers T. A. and Zeitler P. K. (2005) Past, present, and future of thermochronology. *Rev. Mineral. Geochem.* **58**, 1–18.

Reiners P. W. and Farley K. A. (2001) Influence of crystal size on apatite (U–Th)/He thermochronology: an example from the Bighorn Mountains, Wyoming. *Earth Planet. Sci. Lett.* **188**(3–4), 413–420.

Schoene B. and Bowring S. A. (2007) Determining accurate temperature–time paths from U–Pb thermochronology: an example from the Kaapvaal craton, southern Africa. *Geochim. Cosmochim. Acta* **71**(1), 165–185.

Shuster D. L. (2005) ^{4}He/^{3}He thermochronometry: theory, practice, and potential complications. *Rev. Mineral. Geochem.* **58**(1), 181–203.

Shuster D. L. and Farley K. A. (2004) ^{4}He/^{3}He thermochronometry. *Earth Planet. Sci. Lett.* **217**(1–2), 1–17.

Shuster D. L., Flowers R. M. and Farley K. A. (2006) The influence of natural radiation damage on helium diffusion kinetics in apatite. *Earth Planet. Sci. Lett.* **249**(3–4), 148–161.

Spiegel C., Kohn B., Belton D., Berner Z. and Gleadow A. (2009) Apatite (U–Th–Sm)/He thermochronology of rapidly cooled samples: the effect of He implantation. *Earth Planet. Sci. Lett.* **285**(1–2), 105–114.

van Soest M. C., Monteleone B. D., Hodges K. V. and Boyce J. W. (2011) Laser depth profiling studies of helium diffusion in Durango fluorapatite. *Geochim. Cosmochim. Acta* **75**(9), 2409–2419.

Vermeesch P., Seward D., Latkoczy C., Wipf M., Günther D. and Baur H. (2007) Emitting mineral inclusions in apatite, their

effect on (U–Th)/He ages, and how to reduce it. *Geochim. Cosmochim. Acta* **71**(7), 1737–1746.

Watson E. B., Wanser K. H. and Farley K. A. (2010) Anisotropic diffusion in a finite cylinder, with geochemical applications. *Geochim. Cosmochim. Acta* **74**(2), 614–633.

Wolf R., Farley K. and Kass D. (1998) Modeling of the temperature sensitivity of the apatite (U–Th)/He thermochronometer. *Chem. Geol.* **148**(1–2), 105–114.

Associate editor: David L. Shuster